REVIEW

Check for updates

Photodetectors integrating waveguides and semiconductor materials

Xin-Xue Wang,[a] Guang Zeng,[a] Qiu-Jun Yu,[a] Lei Shen,[a] Cai-Yu Shi[a] and Hong-Liang Lu (ID) *[a,b]

Photodetectors integrating substrates and semiconductor materials are increasingly attractive for applications in optical communication, optical sensing, optical computing, and military owing to the unique optoelectronic properties of semiconductor materials. However, it is still a challenge to realize high-performance photodetectors by only integrating substrates and semiconductor materials because of the limitation of incident light in contact with sensitive materials. In recent years, waveguides such as silicon (Si) and silicon nitride (Si_3N_4) have attracted extensive attention owing to their unique optical properties. Waveguides can be easily hetero-integrated with semiconductor materials, thus providing a promising approach for realizing high-performance photodetectors. Herein, we review recent advances in photodetectors integrating waveguides in two parts. The first involves the waveguide types and semiconductor materials commonly used to fabricate photodetectors, including Si, Si_3N_4, gallium nitride, organic waveguides, graphene, and $MoTe_2$. The second involves the photodetectors of different wavelengths that integrate waveguides, ranging from ultraviolet to infrared. These hybrid photodetectors integrating waveguides and semiconductor materials provide an alternative way to realize multifunctional and high-performance photonic integrated chips and circuits.

1. Introduction

Silicon (Si) photodetectors have become very popular in many integrated photonics applications because of their mature CMOS compatibility, outstanding photoelectric characteristics, and unique advantages of high integration density.[1–3] However, because of the inherent material properties of Si, it is very challenging to prepare active photodetectors. Thus, to improve the drawbacks of Si, introducing some other semiconductor materials and integrating them with Si has attracted considerable attention as a promising solution.[4,5] Based on this strategy, in the past decade, researchers have attempted to design and fabricate photodetectors integrating Si with different semiconductor materials, including III–V semiconductor materials,[6,7] germanium,[8] and two-dimensional (2D) semiconductor materials.[9,10] In addition, controlled by self-limiting surface reactions, the atomic layer deposition (ALD) method, a unique preparation process, can be employed to grow 2D semiconductors with high precision, wafer level, and good uniformity and thus widely used in the fields of integrated circuits and optoelectronics.[11] For example, ALD-fabri-

cated photodetectors based on monolayer tungsten trioxide (WO_3) have exhibited outstanding optoelectronic properties.[12,13] However, as the incident light enters a photodetector from the outside of the photodetector, it is difficult to achieve on-chip integration for photodetectors that only integrate Si and semiconductor materials. Thus, to achieve integrated photoelectric chips, photodetectors integrating waveguides and semiconductor materials have attracted increasing attention as a promising solution.[14–16] Fig. 1 shows an outline of this article, which mainly reviews the advanced work on photodetectors integrating waveguides and semiconductor materials, focusing on waveguide materials, waveguide types, semiconductor materials and integrated-waveguide photodetector types. Firstly, various waveguides and semiconductor materials are employed in the fabrication of integrated waveguide photodetectors, including Si, silicon nitride (Si_3N_4), gallium nitride (GaN), organic waveguides, graphene,[17–22] $MoTe_2$, black phosphorus (BP), carbon nanotubes, and palladium selenide ($PdSe_2$).[23–29] Secondly, the waveguide type is further divided into end-coupled waveguide, grating coupled waveguide, and ring waveguide.[30–32] Thirdly, the reported photodetectors with integrated waveguides mainly include infrared (IR) photodetectors, visible (VIS) photodetectors, and ultraviolet (UV) photodetectors.[33–38]

Photodetectors integrating waveguides and semiconductor materials effectively extend the length of the interaction of

[a]State Key Laboratory of ASIC and System, Shanghai Institute of Intelligent Electronics & Systems, School of Microelectronics, Fudan University, Shanghai 200433, China. E-mail: hongliationglu@fudan.edu.cn
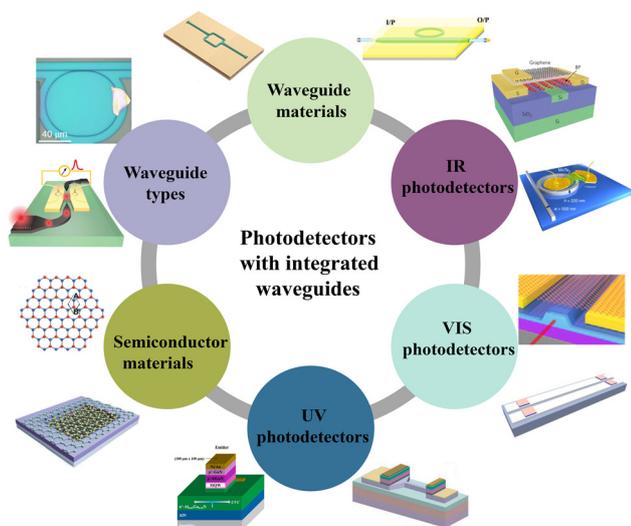*[b]Jiashan Fudan Institute, Jiaxing, Zhejiang Province 314100, China*

Fig. 1 Schematic summary of waveguide materials (reproduced with permission from ref. 21 and 22. Copyright 2022 and 2015, Wiley-VCH and the American Chemical Society, respectively), semiconductor materials (reproduced with permission from ref. 27 and 28. Copyright 2016 and 2020, Wiley-VCH, respectively), waveguide types (reproduced with permission from ref. 31 and 32. Copyright 2020 and 2023, De Gruyter and the American Chemical Society, respectively), and photo-detector types of integrated waveguides (reproduced with permission from ref. 34–38. Copyright 2015, 2020, 2023, 2018, and 2022, Springer Nature, Wiley-VCH, IEEE, and Elsevier, respectively).

light-sensitive materials. Thus, they are expected to achieve many important and extensive applications in the fields of optical communication,[39] imaging,[40] and sensing.[41] In recent years, it has been demonstrated that high-performance photo-detectors integrating waveguides can achieve detection in the ultraviolet (UV) to infrared (IR) region.[42–44] At present, the waveguide materials employed in the fabrication of photo-detectors are mainly Si, Si_3N_4, GaN, lithium cyanate (LN), and ZnO,[45–49] which transmit IR, VIS, and UV light, respectively, due to their inherent properties. Since the first successful exfo-liation of graphene in 2004,[50] two-dimensional (2D) semi-conductor materials have attracted increasing attention in photoelectric detection due to their unique structure and physical properties. Currently, some 2D materials have been used in the field of waveguide photodetectors, including gra-phene,[51] BP,[52] $MoTe_2$,[53] and carbon nanotubes.[54] Further, 2D materials can be conveniently transferred to the waveguide substrate *via* the wet transfer or dry transfer process.[55,56] In this case, lattice matching can be easily achieved. However, due to the small band gap of 2D materials, there is no report on hybrid waveguide/2D material UV photodetectors. In con-trast, there have been reports on high-performance UV photo-detectors integrating waveguides and 3D semiconductor materials.[57] Consequently, photodetectors integrating wave-guides and semiconductor materials are increasingly attractive for many applications.

Herein, we review photodetectors with integrating wave-guide and semiconductor materials. In the second section, the main waveguide materials, waveguide structure, and semi-conductor materials for waveguide photodetectors are intro-duced. In the third section, we review the recent progress on photodetectors with integrated waveguide and semiconductor materials for wavelength bands ranging from UV to IR. Finally, we present conclusions and prospects on the future work of integrated waveguide and semiconductor material photodetectors.

2. Waveguide types and semiconductor materials used for photodetectors

2.1 Waveguide materials and types commonly used for photodetectors

With the development of highly integrated chips, photo-detectors based on waveguides have been further investigated to achieve more compact circuits. Photodetectors integrating waveguides can combine high operational speed and high quantum efficiency simultaneously. This is due to the longer optical absorption length of waveguide-integrated detectors. At this stage, silicon-based waveguides are significantly studied and used to achieve low-loss, low power consumption, small size of the devices and high integrated circuits. Another com-monly used waveguide material, Si_3N_4, is also widely used in the field of photoelectric detection. Researchers have con-ducted some studies on the different structural types of the above-mentioned two commonly used waveguide materials.

Schall *et al.*[58] fabricated photodetectors with an integrated Si waveguide and graphene, which were capable of operating in the 1550 nm band. As shown in Fig. 2a, a 400 nm-wide ridged Si waveguide was produced on 220 nm-thick silicon and covered with a 3 μm buried oxide layer. The fiber loss in the silicon waveguide was only 13.5 dB. The ridge waveguide is a common Si waveguide structure. Another structure of Si wave-guides, *i.e.*, buried waveguide, has also been studied by researchers. Shiue *et al.*[59] prepared hBN/single layer graphene (SLG)/hBN photodetectors with an integrated buried Si wave-guide. As shown in Fig. 2b, the 520 nm-wide Si waveguide was buried among SOI wafers by a shallow channel isolation process. The buried waveguide enabled a flatter interface between the planar waveguide and the 2D material because the SiO_2 layer filling could be used in this structure.

Another common material for waveguides, Si_3N_4, has been used in studies with the two above-mentioned structures. A ridge-based Si_3N_4 waveguide photodetector integrated with graphene was prepared by Gao *et al.*,[30] which could detect 1550 nm IR light. The Si_3N_4 waveguide was obtained by chemi-cal vapor deposition (CVD). As shown in Fig. 2c, the raised spine portion of the Si_3N_4 waveguide is 450 μm long, 1.3 μm wide, and 400 nm high. The SLG directly covers the Si_3N_4 wave-guide and the metal electrode, and the built-in electric field between the metal–graphene junction is beneficial for the sep-aration and transport of photogenerated carriers, and the mul-
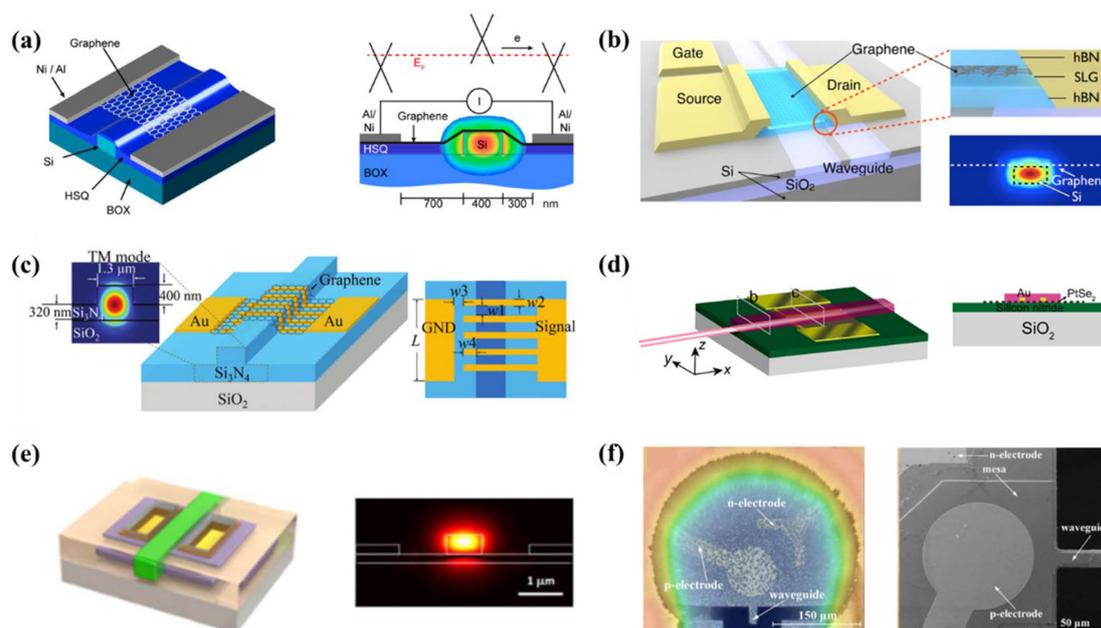
Fig. 2 Waveguide materials and types commonly used in integrated waveguide photodetectors. (a) Photodetector with integrated ridge Si waveguide. Reproduced with permission from ref. 58. Copyright 2014, the American Chemical Society. (b) Photodetector with integrated buried Si waveguide. Reproduced with permission from ref. 59. Copyright 2015, the American Chemical Society. (c) Photodetector with integrated ridge Si_3N_4 waveguide. Reproduced with permission from ref. 30. Copyright 2018, the Royal Society of Chemistry. (d) Photodetector with integrated buried Si_3N_4 waveguide. Reproduced with permission from ref. 64. Copyright 2020, the American Chemical Society. (e) Photodetector with integrated chalcogenide glass waveguide. Reproduced with permission from ref. 66. Copyright 2018, Optical Society of America. (f) Photodetector with integrated InGaN/GaN waveguide. Reproduced with permission from ref. 67. Copyright 2016, Optical Society of America.

tiple metal contacts shorten the transmission distance and time of photogenerated carriers. Wang et al.[64] integrated a buried Si_3N_4 waveguide with $PtSe_2$ photodetector, as shown in Fig. 2d. The use of a ridge waveguide has the tendency to break the 2D material and the deformation at the ridge edges reduces its carrier mobility. Alternatively, buried waveguides can effectively avoid this problem, and thus avoid degrading the properties of the material.

In addition to the common Si and Si_3N_4 waveguides, Li et al.[66] investigated a flexible photodetector based on a chalcogenide glass waveguide, as shown in Fig. 2e. The presence of the flexible waveguide enhances the interaction between matter and light. At 1530 nm, the device has a noise equivalent power of only 0.02 pW $Hz^{1/2}$ and responsivity of 0.35 A W^{-1}, achieving an external quantum efficiency of 28%. As shown in Fig. 2f, a suspended waveguide photodetector with InGaN/GaN multiple quantum wells was fabricated.[67] The prepared photo-

detectors were highly responsive to VIS light at 401 and 435 nm at different voltages, respectively. These results provide a hopeful approach for the development of suspended waveguide photodetectors for various applications in the visible region. To strengthen the comparison between different types of waveguides, we organized a figure of merit table, as shown in Table 1, comparing some parameters such as band gap, refractive index, transmission band, and loss. Waveguide loss is defined as the optical power lost during the transmission of light waves within a waveguide, which has a significant impact on the application of waveguide materials.[64,68] It imposes limitations on the transmission distance of light within the waveguide. Additionally, waveguide loss results in energy wastage, thereby diminishing the overall efficiency of waveguide-based optical communication and sensing systems. According to Table 1, the characteristics of each waveguide material can be clearly distinguished.

Table 1 Comparison of figure of merit of different waveguide materials

Waveguide	Bandgap (eV)	Effective refractive index	Transmission band	Loss	Ref.
Si	~1.1	~3.0 (channel waveguides), ~2.0 (ridge waveguides)	IR (1.3–1.6 µm)	~3.6 dB cm^{-1}	60–63
Si_3N_4	~5–6	~2.0	UV-IR	~4.5 dB cm^{-1}	64, 65
Chalcogenide glass	—	—	IR (1–3.0 µm)	—	66
InGaN/GaN multiple quantum wells	~2.5–3.5	~2.5	UV-blue light	—	67

2.2 Semiconductor materials for photodetectors with integrated waveguides

Since the discovery of graphene in 2004, 2D materials have gradually entered the field of research, opening up new possibilities for the development of high-performance photodetectors. Compared to bulk materials, 2D materials with atomically thin limiting thicknesses are capable of enormous quantum effects, which endow them with unique structures and many excellent capabilities, especially in terms of electronic and optoelectronic properties.[9] 2D materials have high mechanical strength and good flexibility, can be adapted to a wide range of substrate materials, and are well suited for mature CMOS processing, enabling the large-scale integration of silicon photonic structures. Alternatively, 2D materials have high carrier mobility and no dangling bonds, which can very effectively suppress the dark current of photodetectors and realize room temperature detection with high sensitivity and high-speed photoelectric response.[24] Fig. 3 displays the relationship between 2D materials and the corresponding detection bands.[69] According to Fig. 3, it is obvious that some 2D materials have an extremely small intrinsic band gap, such as BP and graphene. In addition, photodetectors integrating these materials are capable of reaching an extremely wide detection spectral range, up to the mid-infrared and even terahertz bands. Thus, the use of 2D materials to achieve a broad-spectrum photoelectric response is very beneficial for the application of these types of photodetectors.

2.2.1 Graphene. The integration of 2D materials onto waveguides is one of the strategies to achieve strong optical interaction. The emergence of 2D materials provides a new option and opportunity to realize high-performance and low-cost broadband photodetectors. The interaction of 2D materials with waveguides results in a higher absorption per unit length than that of the normal incident structure. As a typical representative of 2D materials, the classical graphene has a zero-bandgap, which can generate a large number of carriers through light absorption in a very broad spectrum. This broad

spectrum includes multiple intervals in the UV, visible, short-wave IR, near-IR, mid-IR, far-IR, and terahertz region. 2D materials, including graphene, BP, and tungsten disulfide (WS_2), can be seamlessly integrated with waveguides without significantly affecting the mode fields.[51,52,69] Moreover, graphene materials can be transferred to any substrate without considering lattice mismatch.[70] Simultaneously, the transferred graphene can maintain its excellent electron transport properties. In 2013, Englund et al.[71] demonstrated for the first time a photodetector with integrated waveguide and SLG, as shown in Fig. 4a. This photodetector exhibited a response rate of more than 20 GHz and 12 Gbit per s at zero bias. Schall et al.[72] designed and fabricated a photodetector integrating silicon waveguides and multilayer graphene, which showed good responsivity of 0.18 A W^{-1} to IR light at 1550 nm, as shown in Fig. 4b. Besides pure graphene materials, a very effective modification is to use graphene as a tunable electrode and transition metal sulfide as a photosensitive material, which can exhibit strong light–matter interactions and photon absorption. Based on this property, heterojunction stacks and hybrid devices of graphene and other 2D semiconductors can further enable multifunctional, high-performance photodetectors.

2.2.2 Black phosphorus. Among the 2D materials, BP has attracted increasing attention due to its advantages such as a layered structure with adjustable band gap, better absorption of mid-wave infrared light, and good thermal stability. However, BP still faces oxidation problems in the air and stability issues. Recently, BP has been rediscovered and there has been some research on black phosphorus-based photodetectors. BP has a very narrow direct bandgap structure and it has an anisotropic in-plane laminar lattice structure. These unique advantages give it superior broadband detection characteristics and polarization sensitivity.[19,24] Besides, BP can be integrated on different substrate materials, which makes it quite feasible to fabricate photodetectors with integrated waveguides and BP. In addition to studies on graphene, photodetectors integrating waveguides and BP materials have also been investigated. As shown in Fig. 4d, Lee et al.[73] designed the photodetector integrating an Si waveguide and BP to achieve a photoresponse in the wavelength range of 3.68 to 4.03 μm.

2.2.3 Other 2D semiconductor materials. Compared with graphene and BP materials, transition metal sulfides also have advantages such as excellent optoelectronic properties, structure tunability depending on film thickness, chemical composition and structural diversity. Transition metal dichalcogenides have the additional advantage of being suitable to be used in devices that require electroluminescence. Moreover, the energy band structures of transition metal sulfides vary with the number of layers in the material, thus enabling light detection at different wavelengths. For example, in transition metal sulfides, the transition from an indirect band gap to a direct band gap can be observed by reducing their size from bulk material to the monolayer limit. In addition, 2D carbon nanotubes are often used to prepare photodetectors due to their excellent optoelectronic properties, good thermal conduc-
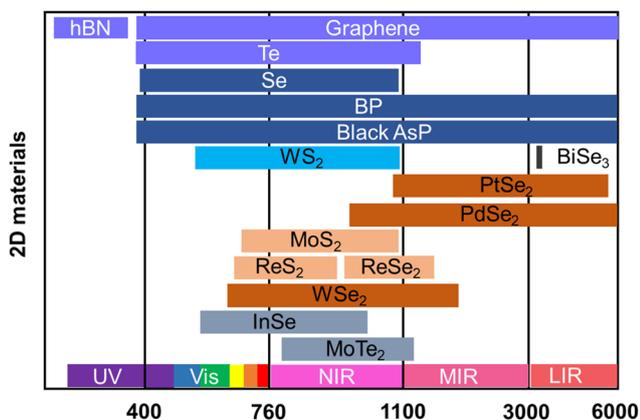

Fig. 3 Relationship between 2D materials and the corresponding detection bands. Reproduced with permission from ref. 69. Copyright 2021, Wiley-VCH.
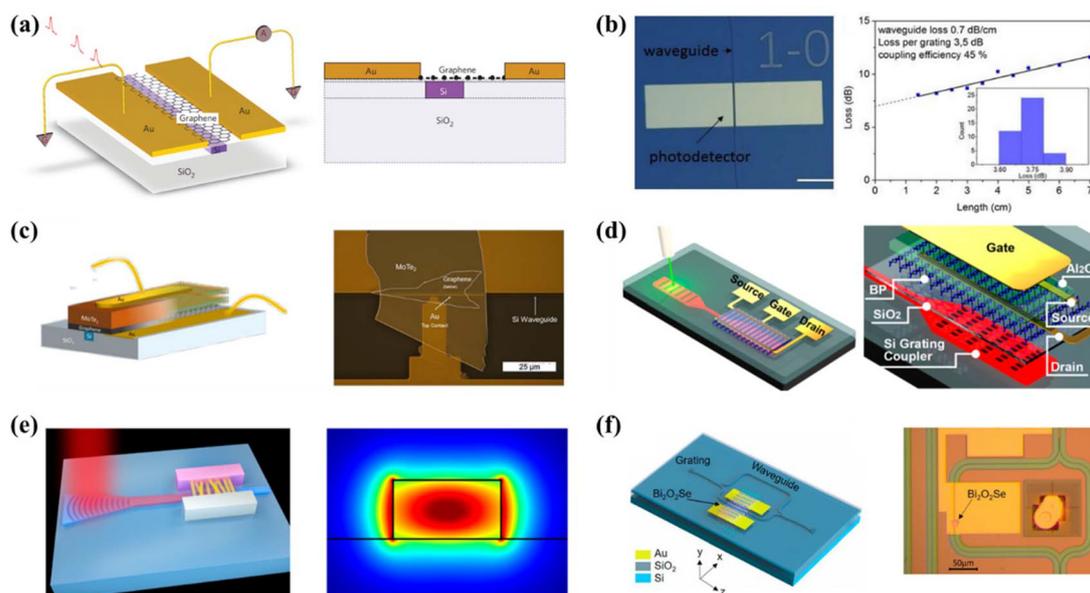
Fig. 4 Semiconductor materials commonly used for integrated waveguide photodetectors. (a) Integrated waveguide photodetector with SLG. Reproduced with permission from ref. 71. Copyright 2013, Springer Nature. (b) Integrated waveguide photodetector with multilayer graphene. Reproduced with permission from ref. 72. Copyright 2018, Optical Society of America. (c) Integrated waveguide photodetector with the graphene/MoTe$_2$ heterojunction. Reproduced with permission from ref. 74. Copyright 2019, Optical Society of America. (d) Integrated waveguide photodetector with BP. Reproduced with permission from ref. 73. Copyright 2018, the American Chemical Society. (e) Integrated waveguide photodetector with carbon nanotubes. Reproduced with permission from ref. 75. Copyright 2020, the American Chemical Society. (f) Integrated waveguide photodetector with Bi$_2$O$_2$Se. Reproduced with permission from ref. 76. Copyright 2021, the American Chemical Society.

tivity, and chemical stability. Recently, 2D multicomponent compounds, such as Bi$_2$O$_2$Se material, have also been used to prepare photodetectors with integrated waveguides. Novotny et al.[74] designed a vertically stacked IR photodetector with integrated Si waveguide and graphene/MoTe$_2$ heterojunction, as shown in Fig. 4c. The photodetectors were obtained by a simple method of mechanical exfoliation and transfer alignment, which can absorb light in the near-IR wavelength range and be applied for photoelectric detection in the telecommunication band. Peng et al.[75] investigated a photodetector based on the integration of carbon nanotubes and waveguides, as shown in Fig. 4e. Carbon nanotubes are very promising materials that are effectively compatible with silicon photonic platforms and other materials. Also, as a direct band gap material, carbon nanotubes are capable of achieving high absorption coefficients over a wide spectral range for fiber optic communication. Based on their ultra-high mobility (100 000 cm^2 V^{-1} s^{-1}) and intrinsic optical response time at room temperature, carbon nanotubes can be used in a wide range of high-speed electronic and optoelectronic devices, including photodetectors. As shown in Fig. 4f, Lin et al. designed and fabricated photodetectors integrating waveguides and Bi$_2$O$_2$Se.[76] Bi$_2$O$_2$Se was first grown on mica by CVD, and then well integrated with the Si waveguide via the transfer method. Meanwhile, the narrow band gap of Bi$_2$O$_2$Se can be used in the study of high-performance near-IR photodetectors.

2.2.4 3D semiconductor materials. The common 2D materials integrated with waveguides are mainly graphene, BP, and transition metal sulfides such as molybdenum sulfide (MoS$_2$), MoTe$_2$, tungsten sulfide (WS$_2$), and boron nitride (BN).[23–25] However, due to the small bandgap of 2D materials, there have been no reports on UV photodetectors integrating waveguides and 2D materials. In contrast, UV photodetectors integrating waveguides and 3D or 1D semiconductor materials, such as Al$_x$Ga$_{1-x}$N and ZnO nanowires, have been reported.[57,77] The reason why Al$_x$Ga$_{1-x}$N and ZnO can achieve UV detection is because their bandgaps (~3.5 eV) are relatively large. These wide-bandgap semiconductors can absorb UV light, enabling UV detection.

3. Waveguide-integrated photo-detectors for different wavelengths

Since the emergence of 2D materials, 2D materials represented by graphene have been increasingly studied in various fields, including gas sensing,[78] medicine,[79] optoelectronics,[80] and composite materials.[81] Especially, 2D materials have received extensive attention in the field of photodetection in recent years due to their unique properties. A photodetector is a light sensor that can convert absorbed light signals into electrical signals and is widely used in optoelectronic systems,[82] communications,[83] aerospace,[84] medical sterilization,[85] fire prevention,[86] the military,[87] and other fields. At present, photodetectors corresponding to different wavelengths play an important role in optical systems in various fields. Therefore,

the development of high-performance photodetectors has received increasing attention. Compared with traditional photodetectors based on 3D semiconductor materials, such as silicon,[88] germanium,[89] and III–V semiconductor materials,[90] photodetectors based on 2D materials are ultra-thin and have high response, outstanding photo-dark current ratio, ultra-high electronic mobility and other advantages. These photodetectors can be classified into UV, visible, and IR photodetectors in terms of their detection wavelength. Further, UV photodetectors are divided into near UV (UVC), far UV (UVB), ultra-short UV (UVA), deep UV (DUV), and extreme UV (EUV) photodetectors according to the wavelength range. Similarly, IR photodetectors can be classified into near-IR (NIR), mid-IR (MIR), and far-IR (FIR) photodetectors according to the wavelength. Alternatively, from the perspective of typical detection principles,[91] photodetectors for 2D materials can be classified into photo-bolometric (PB) effect, photothermoelectric (PTE) effect, photovoltaic (PV) effect, and photoconductive (PC) effect. In the case of the PTE effect, the photocurrent is generated by photon-induced temperature changes in a 2D material. The PB effect refers to the mechanism by which the temperature of the 2D material changes due to light illumination, thereby causing the resistance of the material to change.[92] Regarding the PTE effect, it is a mechanism by which light-induced temperature gradients generate photocurrents.[93] The PV effect is a mechanism by which a 2D material generates additional electron–hole pairs separated by a built-in electric field due to illumination.[94] The PC effect refers to the mechanism by which the electrical conductivity of a 2D material increases due to the photogenerated carriers generated by illumination.[95] The principles of photodetectors corresponding to different 2D materials and different device structures are often not single, but one or several combinations. In addition, from the perspective of the structure of photodetectors, photodetectors based on 2D materials can be divided into two categories. One is a photodetector with 2D materials combined with substrates such as Si, sapphire, and silicon carbide, and the other is a photodetector with 2D materials combined with substrates such as Si, Si_3N_4, and GaN waveguides. Currently, some researchers reviewed the first class of photodetectors.[96] However, it is well known that for 2D materials, taking graphene as an example, it is difficult to achieve high photoresponsivity due to its low absorptivity to incident light (~2.3%). Under this premise, the performance of the first type of photodetectors with the hetero-combination of 2D materials and substrates needs to be further improved due to the limited interaction length between 2D materials and light. As an alternative, the second type of photodetectors integrating 2D materials and waveguides will overcome the above-mentioned problem. In addition, because 2D materials are relatively thin, they can be employed in the evanescent field of waveguide transmission light, and thus the absorption of the incident light by the 2D material can be enhanced, and thus the performance of the photodetector can be improved. In the following part, we review photodetectors for different wavelengths. Furthermore, the parameters corresponding to the photodetectors integrating waveguides and semiconductors are summarized in Table 2.

Table 2 Summary of photodetectors integrating waveguides with semiconductor materials

Materials	Waveguide	Wavelength (μm)	Photodetector type	Bias (V)	Responsivity (A W^{-1})	Bandwidth (GHz)	Ref.
Graphene	Si	1.55	MSM	1	0.108	>20	71
Graphene	Si	1.55	MSM	0	6×10^{-3}	41	58
Graphene	Si	1.31–1.65	MSM	0	0.03	18	105
Graphene	Si	VIS-2.75	Graphene–Si	−1.5	0.13	—	116
Graphene	Si	1.55	MSM	0.4	0.057	7.7	149
Graphene	Si	1.55	MSM	1.2	0.36	42	59
Graphene	Si	1.55	MSM	0	0.035	65	150
Graphene	Si	1.55	MSM	1	1×10^{-3}	76	151
Graphene	Si	1.55	MSM	2	0.273	—	104
Graphene	Si	1.55	MSM	2.2	0.36	110	152
Graphene	Si	6.3–7.1	MSM	0	8×10^{-3}	—	106
Graphene	Si	1.55	FET	−0.3	0.4	40	108
BP	Si	1.55	MSM	0.4	0.135	3	153
BP	Si	2	MSM	0.4	0.307	1.33	154
MoTe$_2$	Si	1.1–1.2	p–n junction	0	1×10^{-3}	—	107
MoTe$_2$	Si	1.3	Graphene–MoTe$_2$	−0.6	0.14	25	60
Graphene	Si$_3$N$_4$	1.55	MSM	0	0.015	30	113
Graphene	Si$_3$N$_4$	1.55	MSM	1	2.36	33	114
Graphene	Si$_3$N$_4$	1.55	p–n junction	0	12.2 (V W^{-1})	42	117
Graphene	Si$_3$N$_4$	1.55	p–n junction	0	6 (V W^{-1})	67	118
PtSe$_2$	Si$_3$N$_4$	1.55	MSM	8	12	35	120
InAlAs/InGaAs	Glass	1.53	MSM	—	0.25	1.4	131
MoS$_2$	Si$_3$N$_4$	0.532	FET	30	0.44	—	123
Si	Si$_3$N$_4$	0.85	p–i–n	20	0.1	—	124
MoS$_2$	Si$_3$N$_4$	0.647	FET	1	1000	—	127
MoSe$_2$	Si$_3$N$_4$	0.78	MoSe$_2$–WS$_2$	2	1	—	128
ZnO	ZnO	0.3–0.7	—	1	—	–	148
Al$_x$Ga$_{1−x}$N	Al$_x$Ga$_{1−x}$N	0.28	p–n junction	—	0.3	—	33

3.1 Waveguide-integrated IR photodetectors

IR photodetectors are very important photodetectors, which have been widely used in various fields of human life, including the military,[97] optical communication,[98] night vision,[99] imaging,[100] thermal imaging cameras,[101] medical treatment,[102] and environmental monitoring.[103] Therefore, 2D materials and waveguide-integrated IR photodetectors have attracted increasing attention in the past decade. In 2013, Kurz *et al.* designed and fabricated a metal–semiconductor–metal (MSM) IR photodetector integrating a waveguide and SLG,[58] as shown in Fig. 2a. This IR photodetector is the first reported photodetector integrating waveguides and 2D materials according to our Web of Science search. The described photodetector with a good responsivity of 0.1 A W^{-1} and 3 dB bandwidth of >20 GHz can be a promising candidate in the field of optical communication (1550 nm). Then, in 2014, another MSM-structured photodetector integrating a waveguide and CVD-grown graphene was reported by Schall *et al.*,[72] as shown in Fig. 4b. The IR photodetector (1550 nm) has a −3 dB bandwidth of 41 GHz and can detect data signals up to 50 Gbit per s. Two years later, Wang *et al.* reported the fabrication of an MSM photodetector (1550 nm) based on graphene and silicon slot waveguides,[104] as shown in Fig. 5a. Compared with the previous

MSM structure detector, the silicon slot waveguide structure can enhance the light intensity and reduce the mode confinement of the transmitted light, which increases the interaction between graphene and incident light. Simultaneously, efficient electron cooling and phonon scattering are lacking in suspended graphene. Consequently, the waveguide achieved an absorption of 0.935 dB μm^{-1} at 1550 nm and a maximum responsivity of 0.273 A W^{-1} in the communication band. Considering a single-communication-band photodetector, Pospischil *et al.* demonstrated an ultra-wide-band complementary metal–oxide semiconductor (CMOS)-compatible IR photodetector based on graphene and Si waveguide,[105] as depicted in Fig. 5b. This photodetector could detect almost all fiber optic telecommunication bands and carry a multi-gigahertz operation. Subsequently, Ma *et al.* designed an MSM photodetector integrating graphene and Si waveguides with a CaF$_2$ substrate as the waveguide cladding,[106] as shown in Fig. 5c. Compared with other waveguide cladding materials, although the photon energy of long-wave infrared (LWIR) is very low, the transmission loss of the Si waveguide based on the CaF$_2$ cladding for LWIR is very low. Therefore, this photodetector showed low loss over a broad LWIR wavelength range of 6.3–7.1 μm. In addition, the photodetector also achieved a broadband responsivity of about 8 mA W^{-1} in the LWIR wavelength at zero bias.
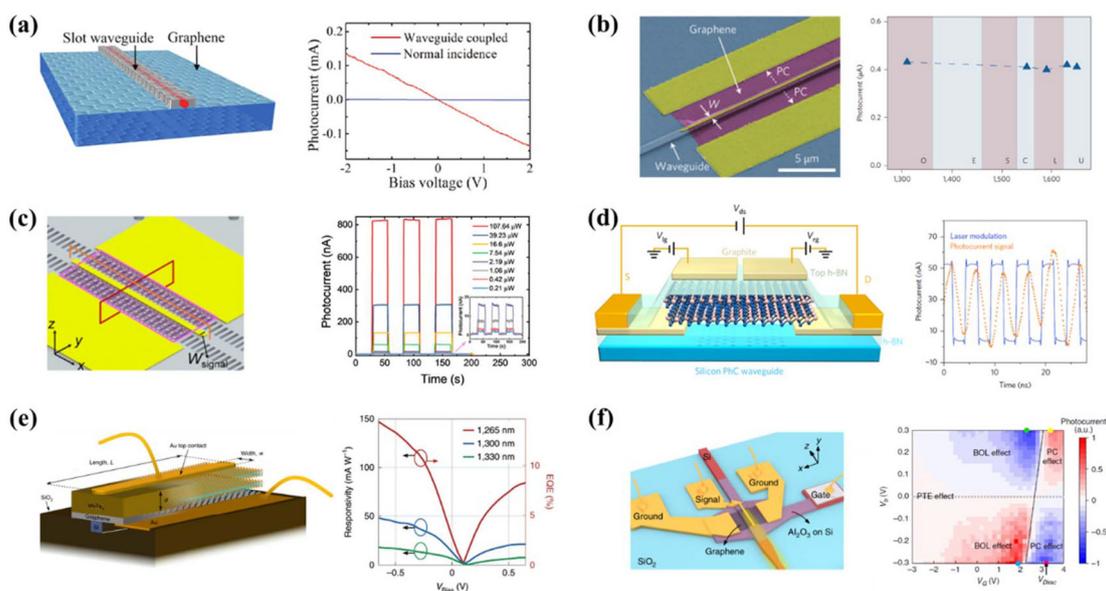

Fig. 5 IR photodetector integrated with Si waveguide and 2D materials. (a) Graphene photodetector with integrated Si slot waveguide. The photocurrent measurement of normal incident and waveguide coupling at 0.5 mW as a function of the bias voltage is shown on the right. Reproduced with permission from ref. 104. Copyright 2016, the Royal Society of Chemistry. (b) Waveguide-integrated graphene photodetector. Photocurrent as a function of the optical communication band is shown on the right. Reproduced with permission from ref. 105. Copyright 2013, Springer Nature. (c) Waveguide-integrated graphene photodetector with CaF$_2$ substrate. The right shows the temporal photoresponses under different incident powers. Reproduced with permission from ref. 106. Copyright 2021, the American Chemical Society. (d) Encapsulated bilayer MoTe$_2$ photodetector is integrated on a silicon photonic-crystal waveguide with a p–n junction. On the right is the dynamic photocurrent under zero bias voltage. Reproduced with permission from ref. 107. Copyright 2017, Springer Nature. (e) Vertical MoTe$_2$–graphene heterostructure photodetector with Si waveguide. The functional relationship between light response and EQE with applied bias at different wavelengths is shown on the right. Reproduced with permission from ref. 60. Copyright 2020, Springer Nature. (f) Si–graphene hybrid plasmonic waveguide photodetector in 1.55 and 2 μm. The measured photocurrent map as V_G and V_b vary is shown on the right. Reproduced with permission from ref. 108. Copyright 2020, Springer Nature.

Notably, it is well known that photodetectors with MSM structures integrated with 2D materials are relatively simple to fabricate. On the one hand, the dark current of these photodetectors is generally large and their response time is relatively long. On the other hand, due to the extended length of the absorption region of the 2D material and the waveguide to transmit light, the photodetector footprint and capacitance will increase, which also hinders the high-speed operation of carriers in the 2D material.[96] The above-mentioned two drawbacks are challenges for realizing high-performance photodetectors. Thus, to overcome these drawbacks, photodetectors such as diodes, heterojunctions, and field effect transistors (FETs) can be considered. Because a diode device can make the dark current of the photodetector very small due to the existence of a depletion region potential barrier, the heterojunction device can shorten the response time of the photodetector due to the built-in electric field of the device. Owing to the regulation of the gate voltage, FET devices can achieve a small dark current, high responsivity, and shortened response time. In 2017, Bie et al. designed and fabricated light-emitting diodes and IR photodetectors (1100 nm) with an integrated Si waveguide and $MoTe_2$,[107] as shown in Fig. 5d. It is well known that for photonic devices, the performance of photodetectors is a challenge faced by researchers. Considering this challenge, the p–n junction photonic device integrating bilayer $MoTe_2$ and Si waveguide can be used as a multifunctional photonic device. Consequently, the detection wavelength of this photodetector covers the range of 1100–1200 nm, and the maximum responsivity occurs at around 1160 nm with 5 mA W^{-1}. Compared with this work, Flöry et al. designed and fabricated a photodetector at telecom wavelengths integrating an Si waveguide and $MoTe_2$–graphene heterojunction,[60] as shown in Fig. 5e. This photodetector achieved a record-high measurement bandwidth (at least 24 GHz) at a bias voltage of −3 V. In addition, Flöry et al. also studied the effect of different thicknesses of $MoTe_2$ flakes on the performance of photodetectors and found that the photodetectors corresponding to thicker $MoTe_2$ flakes have higher photoresponsivity. This is due to the fact that the thicker $MoTe_2$ flakes have higher light absorption. Further, given that the photodetector is a vertical heterostructure device, the photodetector can confine the transmission path length of photogenerated carriers to a few nanometers, thereby achieving a shorter transmission time. Therefore, the photodetector achieved high-speed and high-performance targets with a record bandwidth and a high response of 0.2 A W^{-1} at 1300 nm.

Compared with diode devices and heterojunction devices, although the process of FET devices is more complicated, due to the good control of the gate to the channel, the photogenerated electron–hole pairs can be separated faster under the longitudinal electric field, and thus FET photodetectors have the advantages of small dark current and fast response simultaneously. In 2020, Guo et al. reported the fabrication of an FET photodetector based on an Si waveguide, graphene, and Al_2O_3,[108] as shown in Fig. 5f. The plasmonic waveguide photodetector exhibited an excellent photoelectric performance in

the wavelength range of 1.55 μm and beyond. It is worth noting that the photodetector has many novel designs. Firstly, the Si waveguide is ultra-thin and very wide, enhancing the absorption of transmitted light by graphene. Besides, placing a narrow metal strip on top of the Si waveguide, due to the local surface plasmon resonance effect and the very narrow metal strip, can reduce the absorption of the transmitted light by the metal and enhance the absorption of graphene, and thus the absorption coefficient of graphene can reach 0.23 dB $μm^{-1}$. Further, the presence of gate control improves the performance of the plasmonic waveguide photodetector. Based on these optimized designs, the photodetector exhibited a setting-limited 3 dB bandwidth of >40 GHz and high responsivity of 0.4 A W^{-1} at 1.55 μm and bias voltage of −0.3 V. While operating at 2 μm, the device had a broad 3 dB bandwidth of >20 GHz (setup-limited) and a responsivity of 70 mA W^{-1} at −0.3 V bias. It should be noted that given that graphene is a 0-bandgap 2D material, graphene photodetectors operating in PC mode inevitably have higher dark currents. Alternatively, BP is a direct bandgap material with ∼0.3 eV in bulk and 1.8–2 eV in monolayer form,[109,110] which can be used for broadband photodetection. In addition, compared with graphene, BP has a higher absorption rate.[96] In 2019, Huang et al. presented an FET mid-IR photodetector (3.06–4.03 μm) integrating an Si waveguide and BP,[73] as depicted in Fig. 4d. Under a bias of 1 V, this high-performance photodetector achieved an ultra-high responsivity of 23 A W^{-1} at 3.68 μm and 2 A W^{-1} at 4 μm. Furthermore, the noise equivalent power of this BP photodetector was less than 1 nW $Hz^{-1/2}$ at 1 V and room temperature. The fabrication of these photodetectors integrated with Si waveguides and 2D materials provides a potential way to realize the design and fabrication of on-chip photonic integrated chips for applications in optical communication systems,[39] sensing,[41] imaging,[40] and other fields.

It is worth noting that for electronic devices, Si has a leakage phenomenon because it is a semiconductor material, which will lead to the poor performance of the fabricated photodetectors integrating Si waveguides and 2D materials.[111] Alternatively, given that the band gap of Si materials is relatively small, Si waveguides transmit incident light with wavelengths between 1000 and 1550 nm better.[112] Regarding incident light in other wavelength bands, the loss of Si waveguides increases. Thus, to solve the above-mentioned two problems simultaneously, the Si_3N_4 waveguide is a better alternative. In 2018, Gao et al. designed and fabricated an MSM photodetector integrating Si_3N_4 waveguides and graphene deposited by CVD,[113] as shown in Fig. 6a. Compared with the Si waveguide photodetector, the Si_3N_4 photodetector can block the leakage of carriers into the waveguide and reduce the transmission loss, thereby improving the photoresponse of the photodetector. Further, the IR photodetector innovatively adopts a metal–graphene junction design that increases the interaction between evanescent light and graphene, thereby doubling the responsivity of the photodetector. According to this design, the photodetector achieved a 30 GHz bandwidth and an intrinsic responsivity of 15 mA W^{-1} at ∼1550 nm and
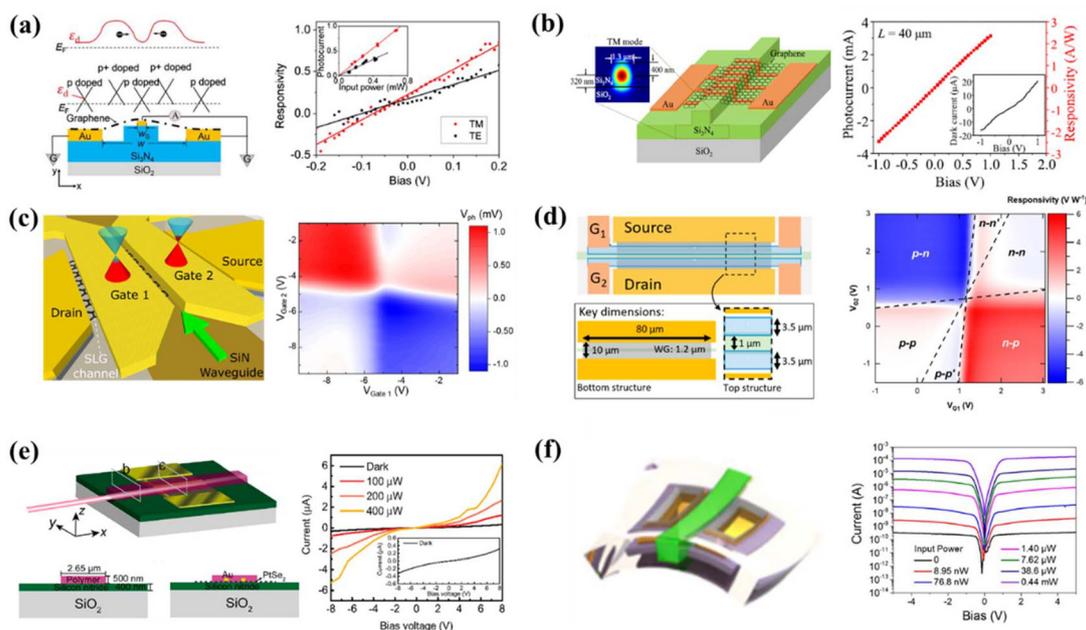
Fig. 6 IR photodetector integrated with different waveguide and semiconductor materials. (a) Si_3N_4–graphene hybrid waveguide photodetector with a signal electrode with a width of w_S and channel width w. The top is the energy band diagram of the photodetector under zero bias and the right is the plot of responsivity as a function of reverse bias at 1550 nm. Reproduced with permission from ref. 113. Copyright 2018, Optical Society of America. (b) A graphene–Si_3N_4 waveguide photodetector with transverse-magnetic mode distribution. The photocurrent and responsivity at an input optical power of 1.314 mW as a function of bias voltage are shown on the right. Reproduced with permission from ref. 114. Copyright 2018, AIP Publishing. (c) The single layer graphene photodetector on Si_3N_4 waveguide with a p−n junction. On the right is the photovoltaic map under zero bias voltage. Reproduced with permission from ref. 117. Copyright 2018, the American Chemical Society. (d) The double single-layer graphene photothermoelectric photodetector on Si_3N_4 waveguide. The simulated photovoltaic map as a function of the voltage applied to the split gate is shown on the right. Reproduced with permission from ref. 118. Copyright 2020, the American Chemical Society. (e) The hybrid $PtSe_2$–SiN photodetector. On the right is the measured I–V curve of the $PtSe_2$ photodetector under dark and different optical powers. Reproduced with permission from ref. 64. Copyright 2020, the American Chemical Society. (f) The flexible waveguide-integrated chalcogenide glass photodetector. The I–V curve of the photodetector under different optical powers is described on the right. Reproduced with permission from ref. 66. Copyright 2018, Optical Society of America.

zero bias, which is comparable to that obtained with the best pristine graphene-based photodetectors. Next, Gao *et al.* improved the metal–graphene junction photodetector and fabricated a grating-like metal contact photodetector (1550 nm) integrating an Si_3N_4 waveguide and graphene,[30] as depicted in Fig. 2c. The resistance–capacitance limited bandwidth of the fabricated device improved because of the relatively small relative permittivity of the Si_3N_4 material. Besides, the IR photodetector innovatively adopts a grating-shaped metal electrode design, which reduces the distance of carrier transmission between the two metal electrodes. Based on this design, a transit time-limited bandwidth of 111 GHz was calculated. Alternatively, for the actual device, it was experimentally found that at 1550 nm, the photodetector has an electro-optical bandwidth of 38 GHz under 0 V bias and an intrinsic responsibility of 13 mA W^{-1} under 0.1 V reverse bias. During the same period, to further improve the performance of the photodetector integrating a waveguide and graphene, Gao *et al.* demonstrated a novel photodetector integrating an Si_3N_4 waveguide and graphene with interdigitated electrode contacts,[114] as shown in Fig. 6b. Based on this design, the photodetector exhibits two detection mechanisms (photovoltaic effect and

photoconductivity effect) under different bias voltages. In the case of the photovoltaic effect, efficient photodetection is mainly achieved by separating photogenerated carriers through the action of a built-in electric field. Given that the region where the metal–graphene junction and band bending exist is small,[115] it is usually much smaller than the distance between the two electrodes. Alternatively, the photogenerated carriers in graphene have a relatively short lifetime,[116] and a large number of carriers is recombined before reaching the contact electrodes. The above-mentioned two problems limit the responsivity of graphene photodetectors. Thus, to overcome these problems, the interdigitated metal contacts employ an interdigital spacing as narrow as 200 nm. At zero bias, the built-in electric field can accelerate the carriers to saturation drift velocity. By increasing the bias voltage, the device can also perform photodetection under the photoconductor mechanism. Consequently, at zero bias and 1550 nm, the high-performance photodetector achieved an electro-optical bandwidth of ~33 GHz. Alternatively, at 1 V bias, the photodetector achieved a responsivity of ~2.36 A W^{-1}. Compared with the MSM photodetector, in 2019, Muench *et al.* demonstrated a split-gate FET photodetector integrating single-layer

graphene, Al_2O_3, and Si_3N_4 waveguide,[117] as depicted in Fig. 6c, where the photodetector mainly works in the telecommunication band. Besides, compared with the large dark current of the MSM device, the photodetector can directly generate a photovoltage with zero dark current through the PTE effect. Further, the design of this Au split gate can not only generate built-in electric fields but also act as surface plasmons to resonate with specific wavelengths of absorbed light. The surface plasmon resonance effect has the function of limiting the absorbed light, thereby increasing the optical field intensity in the graphene channel and the absorption of the transmitted light. Consequently, the high-performance photodetector has the advantages of $\sim$12.2 A W^{-1} external responsivity and a 3 dB bandwidth of $\sim$42 GHz. Mišeikis *et al.* designed and fabricated an FET photodetector integrating a polymer gate dielectric, a graphene channel, and an Si_3N_4 waveguide,[118] as depicted in Fig. 6d. The photodetector adopts a graphene/poly(vinyl alcohol) (PVA)/graphene stack structure, and its detection mechanism is the PTE effect. The use of PVA produces a low charge inhomogeneity of $\sim$8 $\times$ 10^{10} cm^{-2} and a large Seebeck coefficient of $\sim$140 μV K^{-1}, which enhances the PTE effect. In addition, the top split gate is composed of two graphene layers grown by CVD. By applying a gate voltage to each split gate, a p–n junction is created when light absorption in the monolayer graphene channel above the waveguide induces an electron temperature gradient across the junction, enabling photovoltage generation.[119] This photodetector is unaffected by a dark current at $\sim$1550 nm and is currently the fastest graphene photodetector, with a flat frequency response up to 67 GHz without significant loss. Further, this high-performance photodetector is realized on a low-cost, passive photonic platform, and does not rely on nanoscale surface plasmon structures, promising for next-generation communication and data applications.

Due to the low light absorption rate of graphene materials, researchers have been searching for 2D materials to replace graphene.[120] In 2020, Wang *et al.* used transition metal sulfides instead of graphene to design and fabricate MSM photodetectors integrating $PtSe_2$ and Si_3N_4 waveguides,[64] as shown in Fig. 6e. In this design, the researchers innovatively covered $PtSe_2$ with a low-refractive-index polymer. Due to the combined effect of the high-refractive-index Si_3N_4 waveguide and the low-refractive-index polymer waveguide to form bound states in the continuum (BIC),[121,122] the waveguide transmits light into the 2D material and is bound to it, thereby enhancing the mode overlap between the waveguide evanescent field and the 2D material. Consequently, the responsivity of this photodetector at 8 V bias voltage and 1550 nm is $\sim$12 mA W^{-1}. In addition, optical impulse response measurements show a 3 dB bandwidth of 35 GHz, demonstrating the promise of this photodetector integrating Si_3N_4 waveguides and 2D materials for high-speed optoelectronic devices. Hard waveguides such as Si waveguides and Si_3N_4 waveguides are difficult to apply in the fields of wearable devices, flexible consumer electronics, and bendable and stretchable devices. Thus, to overcome the above-mentioned problems, the design and fabrication of flex-ible waveguides have received increasing attention. In 2017, Li *et al.* designed and fabricated an MSM photodetector based on flexible chalcogenide glass (ChG) waveguides and InGaAs,[66] as depicted in Fig. 6f. Consequently, the photodetector exhibited a record optical and mechanical performance measured at 1530 nm with noise equivalent power as low as 0.02 pW $Hz^{1/2}$, linear dynamic range exceeding 70 dB, and 3 dB bandwidth of GHz. In addition, the device could withstand 1000 bending cycles within a sub-millimeter radius without degrading its optoelectronic response. Therefore, the photodetector is expected to become an important device in novel bio-integrated optoelectronic systems, wearable sensors, and flexible consumer electronics.

3.2 Waveguide-integrated VIS photodetectors

VIS light is a common and interesting wavelength band that can be used in biomedical and short-range communication applications.[129,130] VIS photodetectors also play a significant role in these applications.[131] The Si_3N_4 material has good transmittance for the VIS band, and is one of the better candidates as a VIS light waveguide.[124] However, most of the research on photodetectors based on photonic platforms has focused on the IR telecommunication band, and there is still relatively little research on integrated waveguides and semiconductor materials for VIS photodetectors.

Wu *et al.*[123] reported the fabrication of a photodetector based on an Si_3N_4 waveguide. The photodetector integrates the current hot transfer graphene/MoS_2 heterostructure (where the monolayer MoS_2 is obtained by the CVD method). As shown in Fig. 7a, in this structure, photogenerated electron–hole pairs will be generated, and the heterostructure interface will rapidly separate the photogenerated electron–hole pairs. Subsequently, electron transfer to the graphene layer is induced by the built-in electric field. The Fermi energy level of the graphene layer changes in response to the back-gate voltage, which enables the device to achieve an optical responsivity of 440 mA W^{-1} and a rise/fall time of 80/30 ms at 532 nm. This photodetector integrating an optical waveguide with a 2D heterostructure has great potential for future applications in integrated optoelectronic circuits. Selvaraja *et al.*[124] also reported a photodetector integrated on a planar oxide-free Si_3N_4 waveguide SOI platform, which was capable of detecting in the VIS to near-IR wavelength range, which has potential for applications such as biosensing and short-range communication. This is an MSM photodetector with the advantages of high responsivity, low capacitance, low dark current, and high operating speed, as shown in Fig. 7b. The photodetector integrating an Si_3N_4 waveguide with Si can be used in communication applications operating at high speed, providing a fairly reliable sensitivity to the device. Traditional superconducting nanowire single-photodetectors have achieved a high detection efficiency of 98% at a wavelength of 1550 nm, while superconducting nanowire single-photodetectors with integrated waveguides can achieve higher absorption efficiency due to the photons being absorbed in the traveling wave along the propagation direction. As shown in Fig. 7c, Schuck *et al.*[125] demon-
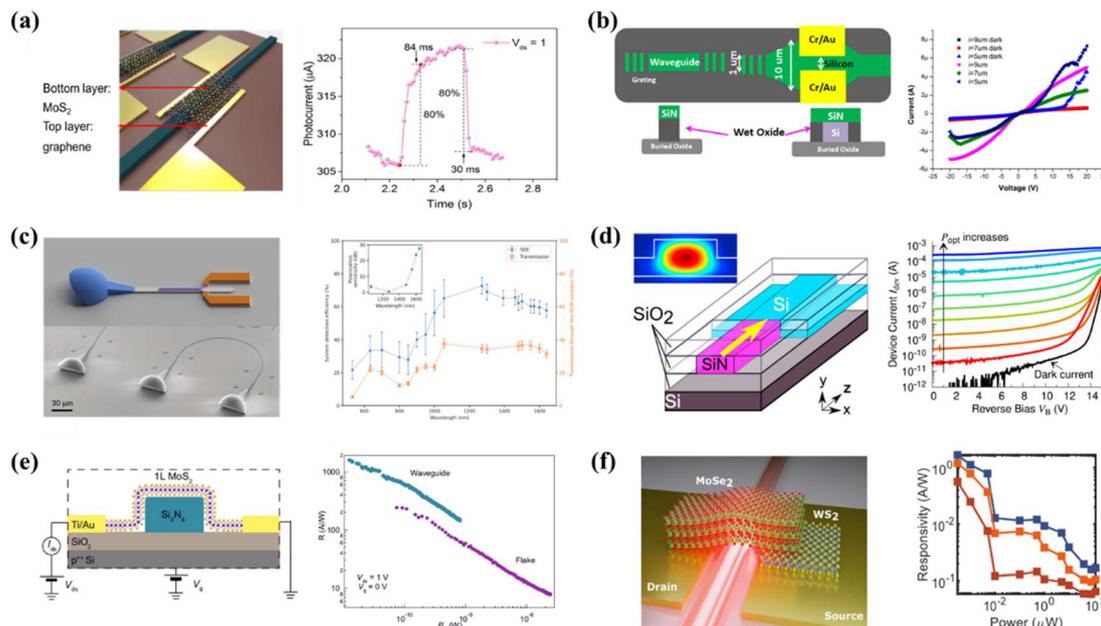
Fig. 7 VIS photodetector integrating Si_3N_4 waveguide with 2D materials. (a) A photodetector with integrated Si_3N_4 waveguide and graphene/MoS_2 heterojunction. The rise/fall time of 80/30 ms at 532 nm is displayed on the right. Reproduced with permission from ref. 123. Copyright 2019, Wiley-VCH. (b) A photodetector with integrated Si_3N_4 waveguide and SOI platform. Photocurrent as a function of voltage is shown on the right. Reproduced with permission from ref. 124. Copyright 2018, SPIE. (c) A photodetector with integrated Si_3N_4 waveguide and nanowires. The right shows the detection efficiencies under different wavelengths. Reproduced with permission from ref. 125. Copyright 2021, AIP Publishing. (d) An avalanche photodetector with integrated Si_3N_4 and Si waveguide. The device current as a function of the reverse bias is shown on the right. Reproduced with permission from ref. 126. Copyright 2021, Springer Nature. (e) VIS photodetector-integrated Si_3N_4 waveguide with 2D MoS_2. The right shows the responsivity under different optical power density with applied bias. Reproduced with permission from ref. 127. Copyright 2019, Published in partnership with FCT NOVA with the support of E-MRS. (f) A VIS photodetector integrated Si_3N_4 waveguide with the $MoSe_2$/WS_2 heterojunction photodiode. The measured responsivity as optical power density is shown on the right. Reproduced with permission from ref. 128. Copyright 2023, under Creative Commons Attribution 4.0 International License.

strated a single photodetector of superconducting nanowires integrated with a single Si_3N_4 waveguide. These researchers integrated a U-shaped superconducting nanowire single-photodetector on top of Si_3N_4. When connected to a fiber *via* a 3D coupler, absorption in a wide band range from 532 to 1640 nm can be achieved with detection efficiencies as high as 22–73%.

Avalanche photodetectors capable of achieving an integrated photonic platform at VIS wavelengths can be used in a variety of miniaturized devices, such as biomedical and underwater imaging, and molecular sensing.[132–134] Leong *et al.*[126] reported the first monolithic avalanche photodetector based on a doped Si ridge waveguide with an integrated Si_3N_4 waveguide. As shown in Fig. 7d, the Si_3N_4 waveguide is used as the input waveguide to reduce the propagation loss of the device in detecting VIS light. The photodetector is capable of detecting 685 nm light at a reverse bias voltage of 20 V. The dark current of all devices can be below 70 pA at a bias voltage of 2 V, indicating that the device is prepared in a quit stable process. In addition, the photodetectors exhibit a dark current of only 1 pA when the waveguide width is 900 nm. Marin *et al.*[127] achieved not only a VIS band photodetector integrating an Si_3N_4 waveguide with 2D MoS_2, but also effective light absorption and photocurrent generation. Fig. 7e displays the structure of this device. The device demonstrates a different

approach from conventional vertical light absorption, with 647 nm VIS light exhibiting near-transverse absorption in the device, which very effectively improves the optical response with an on–off current ratio as high as 6×10^3. Besides, the combination of MoS_2 and hexagonal boron nitride improves the detection speed of the photodetector with a rise/fall time of 13/11 s. Gherabli *et al.*[128] constructed a VIS photodetector integrating an Si_3N_4 waveguide with $MoSe_2$/WS_2 heterojunction photodiode, as shown in Fig. 7f, which exhibits a high responsivity of 1 A W^{-1} at the VIS wavelength of 780 nm. Additionally, the dark current of the device is even reduced to below 50 pA, and the power spectral density of the dark current is as low as $\sim 1 \times 10^{-12}$ A $Hz^{-0.5}$. This research can lay a certain experimental foundation for photodetectors with integrated waveguides and 2D materials in various fields such as optical communication, quantum photonics, and biochemical sensing.

3.3 Waveguide-integrated UV photodetectors

At present, UV photodetectors, as an important part of photodetectors, are mainly used in the military,[135] environmental monitoring,[136] medical field,[137] and space.[138] Due to the short wavelength of UV light, semiconductor materials with a wide bandgap or ultra-wide bandgap are generally required to realize detection, such as ZnO,[139] Ga_2O_3,[140] BN,[141] AlN,[142] and
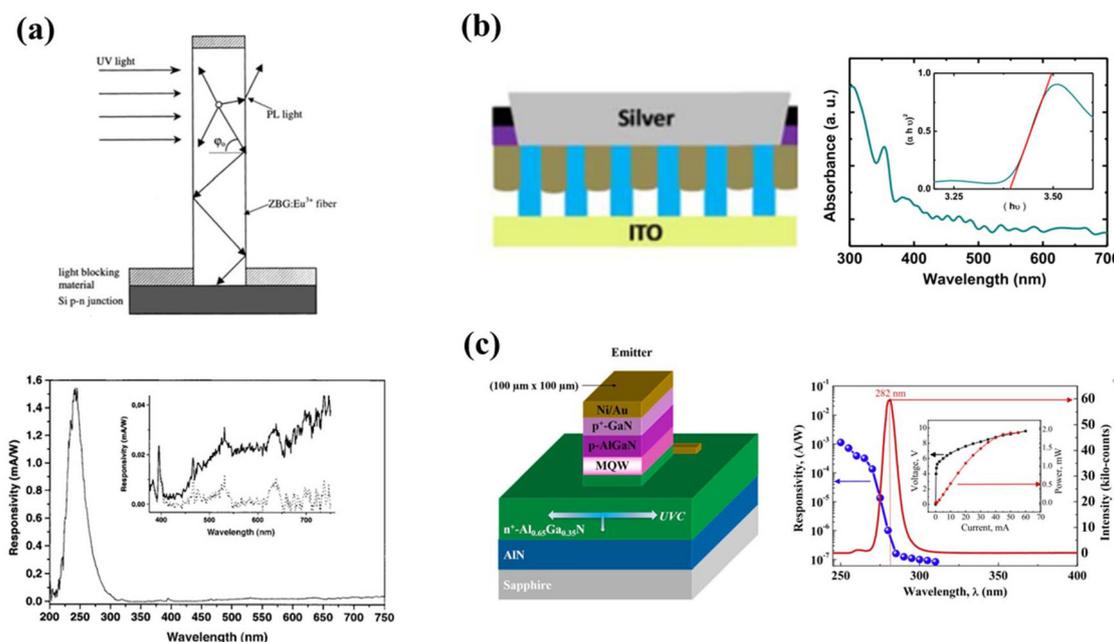
Fig. 8 UV photodetector integrated with different waveguide and semiconductor materials. (a) Eu^{3+}-doped waveguide photodetector with an Si p−n junction. On the right is the spectral photoresponse of the photodetector from UV to IR. Reproduced with permission from ref. 147. Copyright 2001, Wiley-VCH. (b) A vertically grown ZnO nanorod waveguide photodetector based on partially embedded anodized aluminum (AAO) templates. The absorbance curve of ZnO deposited in the AAO template is shown on the right. Reproduced with permission from ref. 148. Copyright 2018, IOP Publishing Ltd. (c) A UVC waveguide photodetector integrating n-type $Al_{0.65}Ga_{0.35}N$ waveguide. On the right is the photodetector and emitter responsivity and emitted power as a function of wavelength. Reproduced with permission from ref. 33. Copyright 2020, the Japan Society of Applied Physics.

diamond.[143] Similarly, to improve the performance of UV photodetectors, integrating UV light-transmitting waveguides with photosensitive semiconductor materials is a promising alternative. However, due to the large photon energy of UV light and the large scattering of UV light, considering the bandgap of the material, there are few waveguide materials that can transmit UV light. Therefore, the current research on UV waveguides is relatively scarce, mainly focusing on waveguide materials such as AlN,[144] Si_3N_4,[145] and ZnO.[146] Consequently, there are currently fewer studies on UV photodetectors integrating UV optical waveguides with semiconductor materials. In 2001, Ivankov et al.[147] designed and fabricated a UV photodetector integrating Eu^{3+}-doped zinc borate glass (ZBG) fibers and Si, as shown in Fig. 8a. The detection principle of the photodetector is to convert the incident UV light into VIS light with a wavelength of 613 nm through the Eu^{3+} doped ZBG fiber. In addition, the device detects UV light through the sensing of VIS light by an Si photodiode. Consequently, the photodetector achieved a photoresponsivity of 3 mA W^{-1} in the UVC band with low power consumption. Further, the maximum sensitivity wavelength of this UV photodetector is in the deep UV range (240–270 nm). It is worth noting that the reason why 3D semiconductor materials are used as sensitive materials for UV photodetectors is that there are relatively few research groups studying photodetectors integrating UV waveguides and semiconductor materials, and these research groups may not have

studied 2D or quasi-2D UV semiconductor materials. Considering that the fiber is relatively difficult to fix, in 2018, Maurya et al.[148] designed and fabricated a vertically grown ZnO nanorod waveguide photodetector based on partially embedded anodized aluminum templates, as shown in Fig. 8b. Compared with bare ZnO nanorods, the photodetector integrating the ZnO nanorod waveguide with hybrid anodized aluminum showed a higher response in the UV band. Consequently, the UV photodetector exhibited a fast response under 365 nm light irradiation, with rise and fall times of ~31 ms and ~85 ms, respectively. In 2020, Floyd et al.[33] designed and fabricated a UVC waveguide photodetector integrating an n-type $Al_{0.65}Ga_{0.35}N$ waveguide and $Al_xGa_{1−x}N$ multiple quantum wells, as depicted in Fig. 8c. The multifunctional photodetector can be used as both a photodetector and a light-emitting diode. Interestingly, the emitter, photodetector, and waveguide share a common epitaxial layer structure. Besides, ~80% of the transmitted light is confined in the n^+-$Al_{0.65}Ga_{0.35}N$ layer, 7% in the AlN cladding, and the remaining 13% in the sapphire substrate. Consequently, the responsivity of this photodetector peaked at 250 nm (1 mA W^{-1}).

4. Conclusion and outlook

Herein, we reviewed the recent studies on photodetectors with integrated waveguides and semiconductor materials for wave-

length bands from the UV to IR region and discussed their potential applications. These applications mainly include optical communications, optical computing, and sensing, as summarized in Fig. 9. With the recent development, the introduction of some semiconductor materials provides alternative opportunities to achieve various active photodetectors on Si substrates because of their fascinating optoelectronic properties. Further, when waveguides and semiconductor materials are integrated, the effect of the light–matter interaction is considerably improved, thereby greatly enhancing the optoelectronic performance of photodetectors. With the rapid development of waveguide technologies, novel and high-performance photodetectors integrating waveguides with semiconductor materials will play an important role in future photoelectric applications. At present, numerous high-speed and high-responsivity waveguide/semiconductor photodetectors have been demonstrated to benefit from the special photoelectric properties of semiconductor materials. However, there are many challenges and bottlenecks preventing the fabrication of higher-performance photodetectors with integrated waveguides and semiconductor materials. Firstly, some 2D materials affect the response of photodetectors integrating waveguides and 2D material due to their shortcomings. For example, graphene materials have low absorptivity and other semiconductor materials such as MoS_2 have low carrier mobility.[23] As shown in Fig. 9, the performance of photodetectors integrating waveguides and semiconductors can be optimized by developing new semiconductor materials or new material structures. Recently, Flöry et al.[60] reported the fabrication of stacked vdW heterostructure photodetector integrating a waveguide and graphene–$MoTe_2$, whose photo-dark-current ratio is almost one order of magnitude better than that of a pure graphene photodetector. In addition, we can design and prepare surface plasmon structures to promote the absorption of incident light transmitted through waveguides by semiconductors, thereby improving the response of photodetectors. Moreover, heterostructures (such as p–n junctions, n–n junctions, and p–i–n junctions) can reduce the dark current and accelerate the separation of photogenerated carriers due to the presence of potential barriers and built-in electric fields, helping to realize high-performance waveguide-integrated photodetectors. Secondly, currently there is no relevant report on UV photodetectors integrating waveguides with quasi-2D or 2D semiconductor materials. A potential solution is to integrate quasi-2D β-Ga_2O_3 or 2D h-BN because these materials have ultra-wide bandgaps suitable for solar blind detection and vacuum UV detection.[155–159] Thirdly, it is also still challenging to realize photodetector arrays integrating waveguides and semiconductor materials with high yield and throughput.[96,160] Searching for advanced growth processes, for example, using the MOCVD method to grow high-quality semiconductor materials, may be the most straightforward way to solve the above-mentioned problem. Lastly, wearable systems are very important for human health, while flexible photodetectors integrating waveguides with semiconductor materials are rarely reported. It is a promising way to fabricate high-performance organic waveguides matched with semiconductor materials by using advanced preparation techniques.

In summary, it is becoming very promising to develop photodetectors on Si substrates through integrated waveguide
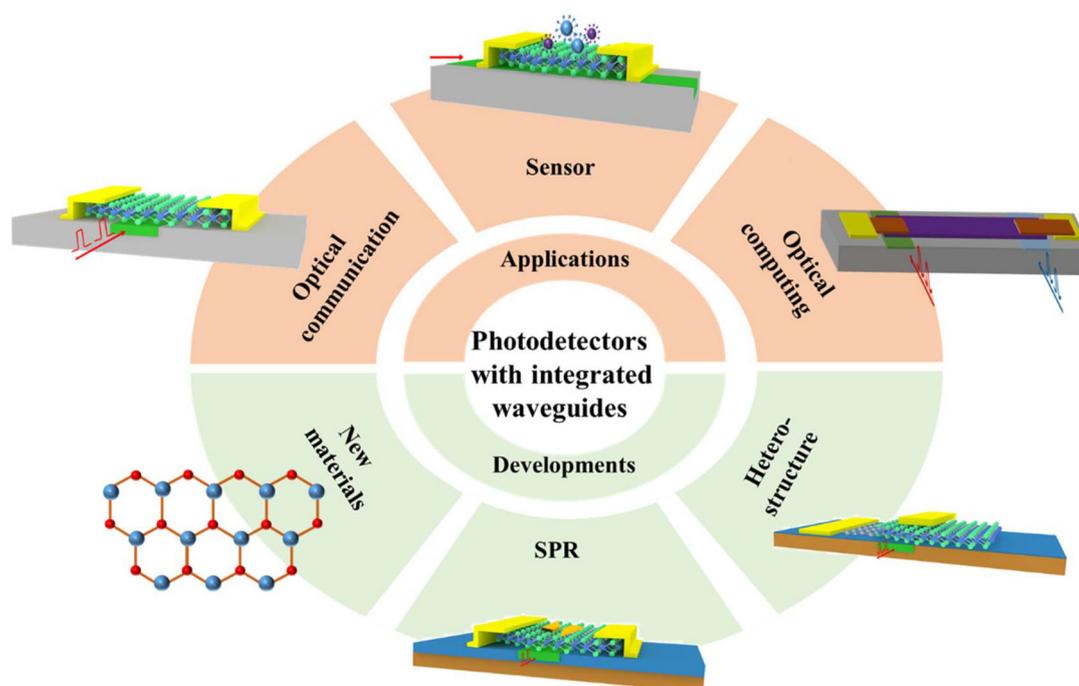

Fig. 9 Schematic summary of the application fields and further development strategies of photodetectors with integrated waveguides.

and semiconductor materials, which can not only compensate for the defects of silicon itself but also realize the design and fabrication of high-performance photodetectors. More importantly, when waveguides and semiconductor materials are integrated, the light–matter interaction can be greatly enhanced, resulting in improved responsivity of the photodetectors. With the rapid development of science and technology, we believe that more advanced photodetectors will appear on new integrated semiconductor materials and waveguide platforms for potential UV-IR applications in optical computing, communications, and biochemical sensing. Therefore, more efforts to realize on-chip photodetectors and apply them to large-scale photonic integrated circuits can be expected in the future.

Author contributions

X.-X. W. and G. Z. contributed equally. X.-X. W. took the lead in conceptualizing and writing the review article. G. Z. contributed towards organizing the summary figures and writing the article. Q.-J. Y. and C.-Y. S. participated in surveying references and organizing figures for each chapter. L. S. was involved in organizing tables and H.-L. L. was involved in supervising and reviewing of the article. All authors read through the article and approved it as the final version.

Conflicts of interest

There are no conflicts to declare.

Acknowledgements

References

1 A. A. Ahmed, M. Hashim, R. Abdalrheem and M. Rashid, *J. Alloys Compd.*, 2019, **798**, 300–310.

2 D. Thomson, A. Zilkie, J. E. Bowers, T. Komljenovic, G. T. Reed, L. Vivien, D. Marris-Morini, E. Cassan, L. Virot and J.-M. Fédéli, *J. Opt.*, 2016, **18**, 073003.

3 M. A. Taubenblatt, *J. Lightwave Technol.*, 2012, **30**, 448–458.

4 N. Youngblood and M. Li, *Nanophotonics*, 2016, **6**, 1205–1218.

5 D. Dai, Y. Yin, L. Yu, H. Wu, D. Liang, Z. Wang and L. Liu, *Front. Optoelectron.*, 2016, **9**, 436–449.

6 A. W. Fang, H. Park, O. Cohen, R. Jones, M. J. Paniccia and J. E. Bowers, *Opt. Express*, 2006, **14**, 9203–9210.

7 H. Park, Y.-h. Kuo, A. W. Fang, R. Jones, O. Cohen, M. J. Paniccia and J. E. Bowers, *Opt. Express*, 2007, **15**, 13539–13546.

8 Y. Ishikawa, K. Wada, D. D. Cannon, J. Liu, H.-C. Luan and L. C. Kimerling, *Appl. Phys. Lett.*, 2003, **82**, 2044–2046.

9 S.-K. Chiu, M.-C. Li, J.-W. Ci, Y.-C. Hung, D.-S. Tsai, C.-H. Chen, L.-H. Lin, K. Watanabe, T. Taniguchi and N. Aoki, *Nanotechnology*, 2023, **34**, 255703.

10 Y. Wang, K. Ding, B. Sun, S.-T. Lee and J. Jie, *Nano Res.*, 2016, **9**, 72–93.

11 S. Zhuiykov, L. Hyde, Z. Hai, M. K. Akbari, E. Kat, C. Detavernier, C. Xue and H. Xu, *Appl. Mater. Today*, 2017, **6**, 44–53.

12 Z. Hai, M. K. Akbari, C. Xue, H. Xu, S. Depuydt and S. Zhuiykov, *Sens. Actuators, B*, 2017, **245**, 954–962.

13 Z. Hai, M. K. Akbari, C. Xue, H. Xu, L. Hyde and S. Zhuiykov, *Appl. Surf. Sci.*, 2017, **405**, 169–177.

14 G. Huang, Y. Hao, Y. D. Jia, J. Guo and H. Zhang, *J. Phys. D: Appl. Phys.*, 2023, **56**, 113001.

15 J. Zhu, J. Cheng, L. Zhang and Q. H. Liu, *Mater. Lett.*, 2017, **186**, 53–56.

16 S. Deckoff-Jones, H. Lin, D. Kita, H. Zheng, D. Li, W. Zhang and J. Hu, *J. Opt.*, 2018, **20**, 044004.

17 A. Chatterjee, S. K. Sikdar and S. K. Selvaraja, *Opt. Lett.*, 2019, **44**, 1682–1685.

18 Y. Lin, Z. Yong, X. Luo, S. S. Azadeh, J. C. Mikkelsen, A. Sharma, H. Chen, J. C. Mak, P. G.-Q. Lo and W. D. Sacher, *Nat. Commun.*, 2022, **13**, 6362.

19 F. Yu, T.-C. Tzu, J. Gao, T. Fatema, K. Sun, P. Singaraju, S. M. Bowers, C. Reyes and A. Beling, *IEEE J. Sel. Top. Quantum Electron.*, 2022, **29**, 1–6.

20 R. B. Taylor, P. E. Burrows and S. R. Forrest, *IEEE Photonics Technol. Lett.*, 1997, **9**, 365–367.

21 H. Ma, J. Wu, Y. Wang, C. Zhong, Y. Ye, M. Wei, R. Yu, Y. Du, B. Tang, C. Sun, Y. Shi, C. Sun, L. Wang, H. Zhu, X. Qiao, L. Li and H. Lin, *Adv. Opt. Mater.*, 2022, **10**, 2201443.

22 C.-L. Wu, Y.-H. Lin, S.-P. Su, B.-J. Huang, C.-T. Tsai, H.-Y. Wang, Y.-C. Chi, C.-I. Wu and G.-R. Lin, *ACS Photonics*, 2015, **2**, 1141–1154.

23 D. Yamashita, H. Machiya, K. Otsuka, A. Ishii and Y. K. Kato, *APL Photonics*, 2021, **6**, 031302.

24 C. Li, R. Tian, X. Chen, L. Gu, Z. Luo, Q. Zhang, R. Yi, Z. Li, B. Jiang and Y. Liu, *ACS Nano*, 2022, **16**, 20946–20955.

25 S. Zhang, Y. Liu, C. Fang, Y. Shao, G. Han, J. Zhang and Y. Hao, *Superlattices Microstruct.*, 2018, **122**, 501–509.

26 J. Jian, J. Wu, C. Zhong, H. Ma, B. Sun, Y. Ye, Y. Luo, M. Wei, K. Lei, R. Liu, Z. Chen, G. Li, H. Dai, R. Tang, C. Sun, J. Li, W. Li, M. Li, H. Lin and L. Li, *ACS Photonics*, 2023, **10**, 3494–3501.

27 X. Li, J. Yu, S. Wageh, A. A. Al-Ghamdi and J. Xie, *Small*, 2016, **48**, 6640–6696.

28 Z. Lu, Y. Xu, Y. Yu, K. Xu, J. Mao, G. Xu, Y. Ma, D. Wu and J. Jie, *Adv. Funct. Mater.*, 2020, **30**, 1907951.

29 J. Wu, H. Ma, C. Zhong, M. Wei, C. Sun, Y. Ye, Y. Xu, B. Tang, Y. Luo, B. Sun, J. Jian, H. Dai, H. Lin and L. Li, *Nano Lett.*, 2022, **22**, 6816–6824.

30 Y. Gao, H. K. Tsang and C. Shu, *Nanoscale*, 2018, **10**, 21851–21856.

31 Y. Ding, Z. Cheng, X. Zhu, K. Yvind, J. Dong, M. Galili, H. Hu, N. A. Mortensen, S. Xiao and L. K. Oxenløwe, *Nanophotonics*, 2020, **9**, 317–325.

32 J. Wu, Y. Ye, J. Jian, X. Yao, J. Li, B. Tang, H. Ma, M. Wei, W. Li, H. Lin and L. Li, *Nano Lett.*, 2023, **23**, 6440–6448.

33 R. Floyd, K. Hussain, A. Mamun, M. Gaevski, G. Simin, M. Chandrashekhar and A. Khan, *Appl. Phys. Express*, 2020, **13**, 022003.

34 N. Youngblood, C. Chen, S. J. Koester and M. Li, *Nat. Photonics*, 2015, **9**, 247–252.

35 R. Maiti, C. Pati, M. Saadi, T. Xie, J. Azadani, B. Uluutku, R. Amin, A. Briggs, M. Miscuglio, D. Thourhout, S. Solares, T. Low, R. Agarwal, S. Bank and V. Sorge, *Nat. Photonics*, 2020, **14**, 578–584.

36 S. Zhu, Y. Zhang, Y. Ren, Y. Wang, K. Zhai, H. Feng, Y. Jin, Z. Lin, J. Feng, S. Li, Q. Yang, N. H. Zhu, E. Pun and C. Wang, *Adv. Photonics Res.*, 2023, **4**, 2300045.

37 K. H. Li, Y. F. Cheung, W. Y. Fu, K. K.-Y. Wong and H. W. Choi, *IEEE J. Sel. Top. Quantum Electron.*, 2018, **24**, 1–6.

38 R. He, N. Liu, Y. Gao, R. Chen, S. Zhang, H. Yuan, Y. Duo, J. Xu, X. Ji, J. Yan, J. Wang, J. Liu, J. Li and T. Wei, *Nano Energy*, 2022, **104**, 107928.

39 R. Soref, *Nat. Photonics*, 2015, **9**, 358–359.

40 Y.-C. Chen, Y.-J. Lu, C.-N. Lin, Y.-Z. Tian, C.-J. Gao, L. Dong and C.-X. Shan, *J. Mater. Chem. C*, 2018, **6**, 5727–5732.

41 W.-C. Lai, S. Chakravarty, Y. Zou and R. T. Chen, *Opt. Lett.*, 2012, **37**, 1208–1210.

42 Y. Wang, W. Yin, Q. Han, X. Yang, H. Ye, Q. Lv and D. Yin, *Chin. Phys. B*, 2016, **25**, 118103.

43 V. Sorianello, M. Balbi, L. Colace, G. Assanto, L. Socci, L. Bolla, G. Mutinati and M. Romagnoli, *Phys. E*, 2009, **41**, 1090–1093.

44 J.-y. Ding, X.-s. Chen, Q. Li, W.-w. Tang, C.-l. Liu, H.-l. Zhen, Y.-l. Jing, H. Wang and W. Lu, *Opt. Quantum Electron.*, 2015, **47**, 2347–2357.

45 J. Fujikata, M. Noguchi, R. Katamawari, K. Inaba, H. Ono, D. Shimura, Y. Onawa, H. Yaegashi and Y. Ishikawa, *Opt. Express*, 2023, **31**, 10732–10743.

46 N. Khongpetch, W. Traiwattanapong, S. Chiangga, P. Limsuwan and P. Chaisakul, *IEEE Access*, 2023, **11**, 19458–19468.

47 H. Zhao, M. Feng, J. Liu, X. Sun, T. Tao, Q. Sun and H. Yang, *Nanophotonics*, 2023, **12**, 111–118.

48 J. Zhang, Y. Li, C. Jiang and Z. Zhao, *IEEE Sens. J.*, 2021, **21**, 20099–20106.

49 H. Wang, S. Jiang, L. Zhang, B. Yu, D. Chen, W. Yang and L. Qian, *Nanoscale*, 2018, **10**, 4727–4734.

50 K. S. Novoselov, A. K. Geim, S. V. Morozov, D.-e. Jiang, Y. Zhang, S. V. Dubonos, I. V. Grigorieva and A. A. Firsov, *Science*, 2004, **306**, 666–669.

51 R. Chen, G. Liu, F. Qiu, Y. Tan and F. Chen, *Opt. Mater. Express*, 2022, **12**, 3614–3620.

52 C. Oliveira, V. Dmitriev, G. Melo and W. Castro, *Microw. Opt. Technol. Lett.*, 2022, **64**, 1170–1175.

53 R. Maiti, C. Patil, M. Saadi, T. Xie, J. Azadani, B. Uluutku, R. Amin, A. Briggs, M. Miscuglio and D. Van Thourhout, *Nat. Photonics*, 2020, **14**, 578–584.

54 H. Zhao, L. Yang, W. Wu, X. Cai, F. Yang, H. Xiu, Y. Wang, Q. Zhang, X. Xin and F. Zhang, *ACS Nano*, 2023, **17**, 7466–7474.

55 X. Li, Y. Zhu, W. Cai, M. Borysiak, B. Han, D. Chen, R. D. Piner, L. Colombo and R. S. Ruoff, *Nano Lett.*, 2009, **9**, 4359–4363.

56 R. A. Hemnani, J. P. Tischler, C. Carfano, R. Maiti, M. H. Tahersima, L. Bartels, R. Agarwal and V. J. Sorger, *2D Mater.*, 2018, **6**, 015006.

57 H. Yang, S. F. Yu, H. Liang, C. Pang, B. Yan and T. Yu, *J. Appl. Phys.*, 2009, **106**, 043102.

58 D. Schall, D. Neumaier, M. Mohsin, B. Chmielak, J. Bolten, C. Porschatis, A. Prinzen, C. Matheisen, W. Kuebart, B. Junginger, W. Templ, A. Giesecke and H. Kurz, *ACS Photonics*, 2014, **1**, 781–784.

59 R.-J. Shiue, Y. Gao, Y. Wang, C. Peng, A. D. Robertson, D. K. Efetov, S. Assefa, F. H. Koppens, J. Hone and D. Englund, *Nano Lett.*, 2015, **15**, 7288–7293.

60 N. Flöry, P. Ma, Y. Salamin, A. Emboras, T. Taniguchi, K. Watanabe, J. Leuthold and L. Novotny, *Nat. Nanotechnol.*, 2020, **15**, 118–124.

61 Y. A. Vlasov and S. J. McNab, *Opt. Express*, 2004, **12**, 1622–1631.

62 S. J. Pearton, J. C. Yang, P. H. Cary, F. Ren, J. Y. Kim, M. J. Tadjer and M. A. Mastro, *Appl. Phys. Rev.*, 2018, **5**, 1.

63 A. V. Krasavin and A. V. Zayats, *Opt. Express*, 2010, **18**, 11791–11799.

64 Y. Wang, Z. Yu, Z. Zhang, B. Sun, Y. Tong, J.-B. Xu, X. Sun and H. K. Tsang, *ACS Photonics*, 2020, **7**, 2643–2649.

65 S. H. Badri and M. M. Gilarlue, *Opt. Commun.*, 2020, **460**, 125089.

66 L. Li, H. Lin, Y. Huang, R.-J. Shiue, A. Yadav, J. Li, J. Michon, D. Englund, K. Richardson and T. Gu, *Optica*, 2018, **5**, 44–51.

67 W. Yuan, Y. Xu, X. Gao, B. Zhu, W. Cai, G. Zhu, Y. Yang and Y. Wang, *Opt. Mater. Express*, 2016, **6**, 2366–2373.

68 D. X. Dai, J. Bauters and J. E. Bowers, *Light: Sci. Appl.*, 2012, **1**, e1.

69 Q. Qiu and Z. Huang, *Adv. Mater.*, 2021, **33**, 2008126.

70 G. Zeng, M.-R. Zhang, Y.-C. Chen, X.-X. Li, D.-B. Chen, C.-Y. Shi, X.-F. Zhao, N. Chen, T.-Y. Wang and D. W. Zhang, *Mater. Today Phys.*, 2023, **33**, 101042.

71 X. Gan, R.-J. Shiue, Y. Gao, I. Meric, T. F. Heinz, K. Shepard, J. Hone, S. Assefa and D. Englund, *Nat. Photonics*, 2013, **7**, 883–887.

72 D. Schall, E. Pallecchi, G. Ducournau, V. Avramovic, M. Otto and D. Neumaier, Opt. Fiber Commun. Conf. and Expo., IEEE, 2018, pp. 1–3.

73 L. Huang, B. Dong, X. Guo, Y. Chang, N. Chen, X. Huang, W. Liao, C. Zhu, H. Wang and C. Lee, *ACS Nano*, 2018, **13**, 913–921.

74 P. Ma, N. Flöry, Y. Salamin, A. Emboras, T. Taniguchi, K. Watanabe, L. Novotny and J. Leuthold, Conf. on Lasers and Electro-Optics, IEEE, 2019, pp. 1–2.

75 Z. Ma, L. Yang, L. Liu, S. Wang and L.-M. Peng, *ACS Nano*, 2020, **14**, 7191–7199.

76 J. Wu, M. Wei, J. Mu, H. Ma, C. Zhong, Y. Ye, C. Sun, B. Tang, L. Wang, J. Li, X. Xu, B. Liu, L. Li and H. Lin, *ACS Nano*, 2021, **15**, 15982–15991.

77 S. M. Nawaz, M. I. Niass, Y. Wang, Z. Xing, F. Wang and Y. Liu, *Superlattices Microstruct.*, 2020, **145**, 106643.

78 L. Zhang, K. Khan, J. Zou, H. Zhang and Y. Li, *Adv. Mater. Interfaces*, 2019, **6**, 1901329.

79 M. Derakhshi, S. Daemi, P. Shahini, A. Habibzadeh, E. Mostafavi and A. A. Ashkarran, *J. Funct. Biomater.*, 2022, **13**, 27.

80 G. Kim, S. Song and D. Jariwala, *Mater. Res. Lett.*, 2023, **11**, 327–346.

81 E. Lacatus, *Mater. Today: Proc.*, 2018, **5**, 17484–17491.

82 E. Wu, D. Wu, C. Jia, Y. Wang, H. Yuan, L. Zeng, T. Xu, Z. Shi, Y. Tian and X. Li, *ACS Photonics*, 2019, **6**, 565–572.

83 P. Grant, S. Laframboise, R. Dudek, M. Graf, A. Bezinger and H. Liu, *Electron. Lett.*, 2009, **45**, 1.

84 E. W. Taylor, T. Zeng, D. Wood and R. O. Claus, *Enabl. Photon. Technol. Aerosp. Appl. VI*, 2004, vol. 5435, pp. 164–170.

85 U. Varshney, N. Aggarwal and G. Gupta, *J. Mater. Chem. C*, 2022, **10**, 1573–1593.

86 X. Guo, L. Tang, J. Xiang, R. Ji, K. Zhang, S. K. Lai, J. Zhao, J. Kong and S. P. Lau, *AIP Adv.*, 2016, **6**, 055318.

87 Z. Alaie, S. M. Nejad and M. Yousefi, *Mater. Sci. Semicond. Process.*, 2015, **29**, 16–55.

88 M.-K. Lee, C.-H. Chu, Y.-H. Wang and S. Sze, *Opt. Lett.*, 2001, **26**, 160–162.

89 J. Wang and S. Lee, *Sensors*, 2011, **11**, 696–718.

90 P. Binetti, X. Leijtens, T. De Vries, Y. Oei, L. Di Cioccio, J.-M. Fedeli, C. Lagahe, J. Van Campenhout, D. Van Thourhout and P. Van Veldhoven, *IEEE Photonics J.*, 2010, **2**, 299–305.

91 F. Koppens, T. Mueller, P. Avouris, A. Ferrari, M. Vitiello and M. Polini, *Nat. Nanotechnol.*, 2014, **9**, 780–793.

92 M. Freitag, T. Low, F. Xia and P. Avouris, *Nat. Photonics*, 2013, **7**, 53–59.

93 X. Xu, N. M. Gabor, J. S. Alden, A. M. Van Der Zande and P. L. McEuen, *Nano Lett.*, 2010, **10**, 562–566.

94 E. C. Peters, E. J. Lee, M. Burghard and K. Kern, *Appl. Phys. Lett.*, 2010, **97**, 193102.

95 Z. Chen, Z. Cheng, J. Wang, X. Wan, C. Shu, H. K. Tsang, H. P. Ho and J. B. Xu, *Adv. Opt. Mater.*, 2015, **3**, 1207–1214.

96 J. Li, C. Liu, H. Chen, J. Guo, M. Zhang and D. Dai, *Nanophotonics*, 2020, **9**, 2295–2314.

97 N. Ilyas, D. Li, Y. Song, H. Zhong, Y. Jiang and W. Li, *Sensors*, 2018, **18**, 4163.

98 A. K. Dutta, R. Olah, G. Mizuno and N. K. Dhar, *Opt. Metro Netw. Short-Haul Syst. III*, 2011, vol. 7959, p. 795906.

99 Q. Wang, Y. Zhang and Z. Wei, *Chin. J. Chem.*, 2023, **41**, 958–978.

100 J. Miao, B. Song, Z. Xu, L. Cai, S. Zhang, L. Dong and C. Wang, *Small*, 2018, **14**, 1702082.

101 H. Schneider, P. Koidl, M. Walther, J. Fleißner and J. Ziegler, *TM, Tech. Mess.*, 1999, **66**, 344–349.

102 M. Fauci, R. Breiter, W. Cabanski, W. Fick, R. Koch, J. Ziegler and S. Gunapala, *Infrared Phys. Technol.*, 2001, **42**, 337–344.

103 Y. Zhang, L. Tang and K. S. Teng, *Nanotechnology*, 2020, **31**, 304002.

104 J. Wang, Z. Cheng, Z. Chen, X. Wan, B. Zhu, H. K. Tsang, C. Shu and J. Xu, *Nanoscale*, 2016, **8**, 13206–13211.

105 A. Pospischil, M. Humer, M. M. Furchi, D. Bachmann, R. Guider, T. Fromherz and T. Mueller, *Nat. Photonics*, 2013, **7**, 892–896.

106 Y. Ma, Y. Chang, B. Dong, J. Wei, W. Liu and C. Lee, *ACS Nano*, 2021, **15**, 10084–10094.

107 Y.-Q. Bie, G. Grosso, M. Heuck, M. M. Furchi, Y. Cao, J. Zheng, D. Bunandar, E. Navarro-Moratalla, L. Zhou and D. K. Efetov, *Nat. Nanotechnol.*, 2017, **12**, 1124–1129.

108 J. Guo, J. Li, C. Liu, Y. Yin, W. Wang, Z. Ni, Z. Fu, H. Yu, Y. Xu and Y. Shi, *Light: Sci. Appl.*, 2020, **9**, 29.

109 L. Li, Y. Yu, G. J. Ye, Q. Ge, X. Ou, H. Wu, D. Feng, X. H. Chen and Y. Zhang, *Nat. Nanotechnol.*, 2014, **9**, 372–377.

110 H. Liu, A. T. Neal, Z. Zhu, Z. Luo, X. Xu, D. Tománek and P. D. Ye, *ACS Nano*, 2014, **8**, 4033–4041.

111 M. Liu, X. Yin, E. Ulin-Avila, B. Geng, T. Zentgraf, L. Ju, F. Wang and X. Zhang, *Nature*, 2011, **474**, 64–67.

112 D. Dai and J. E. Bowers, *Nanophotonics*, 2014, **3**, 283–311.

113 Y. Gao, G. Zhou, N. Zhao, H. K. Tsang and C. Shu, *Opt. Lett.*, 2018, **43**, 1399–1402.

114 Y. Gao, L. Tao, H. K. Tsang and C. Shu, *Appl. Phys. Lett.*, 2018, **112**, 211107.

115 S. D. Sarma, S. Adam, E. Hwang and E. Rossi, *Rev. Mod. Phys.*, 2011, **83**, 407.

116 X. Wang, Z. Cheng, K. Xu, H. K. Tsang and J.-B. Xu, *Nat. Photonics*, 2013, **7**, 888–891.

117 J. E. Muench, A. Ruocco, M. A. Giambra, V. Miseikis, D. Zhang, J. Wang, H. F. Watson, G. C. Park, S. Akhavan and V. Sorianello, *Nano Lett.*, 2019, **19**, 7632–7644.

118 V. Mišeikis, S. Marconi, M. A. Giambra, A. Montanaro, L. Martini, F. Fabbri, S. Pezzini, G. Piccinini, S. Forti and B. Terrés, *ACS Nano*, 2020, **14**, 11190–11204.

119 N. M. Gabor, J. C. Song, Q. Ma, N. L. Nair, T. Taychatanapat, K. Watanabe, T. Taniguchi, L. S. Levitov and P. Jarillo-Herrero, *Science*, 2011, **334**, 648–652.

120 T. Zhu, Y. Zhang, X. Wei, M. Jiang and H. Xu, *Front. Phys.*, 2023, **18**, 33601.

121 Z. Yu, X. Xi, J. Ma, H. K. Tsang, C.-L. Zou and X. Sun, *Optica*, 2019, **6**, 1342–1348.

122 Z. Yu and X. Sun, *Light: Sci. Appl.*, 2020, **9**, 1.

123 Z. Wu, T. Zhang, Y. Chen, Y. Zhang and S. Yu, *Phys. Status Solidi RRL*, 2019, **13**, 1800338.

124 A. Chatterjee and S. K. Selvaraja, *Opt. Compon. Mater. XV*, 2018, vol. 10528, pp. 160–165.

125 M. A. Wolff, F. Beutel, J. Schütte, H. Gehring, M. Häußler, W. Pernice and C. Schuck, *Appl. Phys. Lett.*, 2021, **118**, 154004.

126 S. Yanikgonul, V. Leong, J. R. Ong, T. Hu, S. Y. Siew, C. E. Png and L. Krivitsky, *Nat. Commun.*, 2021, **12**, 1834.

127 J. G. Marin, D. Unuchek, K. Watanabe, T. Taniguchi and A. Kis, *npj 2D Mater. Appl.*, 2019, **3**, 14.

128 R. Gherabli, S. Indukuri, R. Zektzer, C. Frydendahl and U. Levy, *Light: Sci. Appl.*, 2023, **12**, 60.

129 T. Komine and M. Nakagawa, *IEEE Trans. Consum. Electron.*, 2004, **50**, 100–107.

130 X. Shu, L. Beckmann and H. F. Zhang, *J. Biomed. Opt.*, 2017, **22**, 121707–121707.

131 H. Zhang, D. Wei, X. Song, Z. Xu, F. Wang, H. Li, W. Sun, Z. Dai, Y. Ren and Y. Ye, *Nanotechnology*, 2023, **34**, 185205.

132 V. Gruev, J. Van der Spiegel and N. Engheta, *Opt. Express*, 2010, **18**, 19292–19303.

133 J. Miao and C. Wang, *Nano Res.*, 2021, **14**, 1878–1888.

134 Y. Yuan, B. Tossoun, Z. Huang, X. Zeng, G. Kurczveil, M. Fiorentino, D. Liang and R. G. Beausoleil, *J. Semicond.*, 2022, **43**, 021301.

135 J. Yang, K. Liu, X. Chen and D. Shen, *Prog. Quantum Electron.*, 2022, **83**, 100397.

136 G. Shang, L. Tang, G. Wu, S. Yuan, M. Jia, X. Guo, X. Zheng, W. Wang, B. Yue and K. S. Teng, *Sensors*, 2023, **23**, 2741.

137 Y. Liu, Z. C. Li, P. F. Wang, F. Huang and J. L. Sun, *J. Infrared Millimeter Waves*, 2023, **42**, 169–187.

138 E. Monroy, F. Omnès and F. Calle, *Semicond. Sci. Technol.*, 2003, **18**, R33.

139 J. Hu, J. Chen, T. Ma and Z. Li, *Nanotechnology*, 2023, **34**, 232002.

140 L. Qu, J. Ji, X. Liu, Z. Shao, M. Cui, Y. Zhang, Z. Fu, Y. Huang, G. Yang and W. Feng, *Nanotechnology*, 2023, **34**, 225203.

141 N. R. Abdullah, B. J. Abdullah, C.-S. Tang and V. Gudmundsson, *Mater. Sci. Eng., B*, 2023, **288**, 116147.

142 T. Li, Y. Lu and Z. Chen, *Nanomaterials*, 2022, **12**, 4169.

143 M. Feng, P. Jin, X. Meng, P. Xu, X. Huo, G. Zhou, P. Qu, J. Wu and Z. Wang, *J. Phys. D: Appl. Phys.*, 2022, **55**, 404005.

144 M. M. Satter, Z. Lochner, T.-T. Kao, Y.-S. Liu, X.-H. Li, S.-C. Shen, R. D. Dupuis and P. D. Yoder, *IEEE J. Quantum Electron.*, 2014, **50**, 166–173.

145 A. Z. Subramanian, E. Ryckeboer, A. Dhakal, F. Peyskens, A. Malik, B. Kuyken, H. Zhao, S. Pathak, A. Ruocco and A. De Groote, *Photonics Res.*, 2015, **3**, B47–B59.

146 E. S. Leong, S. F. Yu, A. Abiyasa and S. P. Lau, *Appl. Phys. Lett.*, 2006, **88**, 091116.

147 A. Ivankov and W. Bauhofer, *Phys. Status Solidi A*, 2001, **185**, 145–151.

148 M. R. Maurya and V. Toutam, *Nanotechnology*, 2018, **30**, 085704.

149 N. Youngblood, Y. Anugrah, R. Ma, S. J. Koester and M. Li, *Nano Lett.*, 2014, **14**, 2741–2746.

150 S. Schuler, D. Schall, D. Neumaier, L. Dobusch, O. Bethge, B. Schwarz, M. Krall and T. Mueller, *Nano Lett.*, 2016, **16**, 7107–7112.

151 D. Schall, C. Porschatis, M. Otto and D. Neumaier, *J. Phys. D: Appl. Phys.*, 2017, **50**, 124004.

152 Y. Ding, Z. Cheng, X. Zhu, K. Yvind, J. Dong, M. Galili, H. Hu, N. A. Mortensen, S. Xiao and L. K. Oxenløwe, *Nanophotonics*, 2020, **9**, 317–325.

153 C. Chen, N. Youngblood, R. Peng, D. Yoo, D. A. Mohr, T. W. Johnson, S.-H. Oh and M. Li, *Nano Lett.*, 2017, **17**, 985–991.

154 Y. Yin, R. Cao, J. Guo, C. Liu, J. Li, X. Feng, H. Wang, W. Du, A. Qadir and H. Zhang, *Laser Photonics Rev.*, 2019, **13**, 1900032.

155 S. Pu, Y. Ou, M. Cai, Y. Xia and Z. Wu, *Mater. Lett.*, 2023, **342**, 134283.

156 Y.-C. Lu, Z.-F. Zhang, X. Yang, G.-H. He, C.-N. Lin, X.-X. Chen, J.-H. Zang, W.-B. Zhao, Y.-C. Chen and L.-L. Zhang, *Nano Res.*, 2022, **15**, 7631–7638.

157 C. Zhang, K. Liu, Q. Ai, X. Huang, X. Chen, Y. Zhu, J. Yang, Z. Cheng, B. Li and L. Liu, *J. Phys. Chem. C*, 2022, **126**, 21839–21846.

158 W. Zheng, R. Lin, Z. Zhang and F. Huang, *ACS Appl. Mater. Interfaces*, 2018, **10**, 27116–27123.

159 Y. Li, J. Guo, W. Zheng and F. Huang, *Appl. Phys. Lett.*, 2020, **117**, 023504.

160 Y. Liu, Y. Huang and X. Duan, *Nature*, 2019, **567**, 323–333.